Modified Symbol Timing Offset Estimation for OFDM over Frequency Selective Channels

Qi Wang, Michal Šimko and Markus Rupp

Institute of Telecommunications, Vienna University of Technology
Gusshausstrasse 25/389, A-1040 Vienna, Austria
Email: {qwang, msimko, mrupp}@nt.tuwien.ac.at
Web: http://www.nt.tuwien.ac.at/rapid-prototyping

***Abstract*—This paper deals with the symbol timing issue of an OFDM system in frequency selective fading scenarios. A modified symbol timing offset estimator based on an energy transition metric is proposed. This metric can also be applied to estimate the maximum channel delay spread. Benefitting from the knowledge of the maximum channel delay spread, the modified estimator shows its advantage in a relatively low SNR regime. Compared to the original, the modified algorithm is able to acquire the symbol timing correctly in a relatively low SNR region.**

I. Introduction

Orthogonal Frequency Division Multiplexing (OFDM) has become a dominant physical layer technique in modern wireless communication systems such as WiMAX and UMTS Long Term Evolution (LTE) [1, 2]. Given the advantage of dividing the available bandwidth into narrow subchannels, OFDM enables high data rate transmission in frequency selective fading scenarios. The guard interval at the beginning of each OFDM symbol provides certain tolerance to symbol timing errors introduced by multi-path channels. However, once a Symbol Timing Offset (STO) occurs outside the guard interval, the system performance degrades due to the Inter-Carrier Interference (ICI) and Inter-Symbol Interference (ISI) [3, 4].

The literature on STO and Carrier Frequency Offset (CFO) estimation falls into two categories: data-aided and non-data-aided. Data-aided methods estimate the timing and frequency offsets based on autocorrelation [5–7] where usually a repetitive pattern in the preamble is required. On the other hand, non-data-aided methods, either rely on the guard interval, namely the Cyclic Prefix (CP) [8, 9], or exploit the cyclostationarity of the OFDM signal. Usually, these methods require the knowledge of either the pulse shaping filter [10] or the maximum delay spread [11] instead of a pre-defined preamble.

We are interested in the non-data-aided methods based on the CP [8, 9] since it can be applied to the systems which do not have a preamble defined. However, in a Non-Line-Of-Sight (NLOS) multi-path scenario, the autocorrelation based method [8] exhibits the critical drawback that the signal arriving from the strongest path is identified instead of the one who arrives first. Such a "late" detection introduces ISI from the successive OFDM symbol. In [9], a blind coarse timing offset estimator based on an energy transition metric is proposed. In contrast to the autocorrelation metric, this technique is able to estimate the STO in a deep frequency selective fading scenario at a high Signal-to-Noise Ratio (SNR), while in the low SNR regime, the error probability stays rather high.

In this paper, we modify the energy transition metric proposed in [9] in order to improve further the estimation performance in the low SNR regime. We utilize the same metric to estimate the channel maximum delay spread, with which the estimation performance is boosted.

The paper is organized as follows. In Section II, we introduce the system model and elaborate the modified algorithm after a brief review of the original method. In Section III, we discuss several aspects of the modified estimator such as optimal parameter selection and an extension to multiple antenna receivers. Simulation results are presented in Section IV. Section V concludes the report.

II. STO Estimation Algorithms

In this section, firstly we describe the system model. Secondly, the STO estimator proposed in [9] is reviewed. Eventually, the modified energy transition metric is proposed.

A. System Model

An OFDM symbol in the time domain consists of N time samples of total duration $T_\mathrm{s} = NT$ and N_g samples as CP of duration $T_\mathrm{g} = N_\mathrm{g}T$. We denote the transmitted signal as s_n and the received as r_n where n is the time index.

We consider a discrete tapped delay line channel model with its impulse response written as

$$h_n = \sum_{l=0}^{L} a_l \cdot \delta_K(n-l), \tag{1}$$

where L is the normalized maximum channel delay and a_l the complex-valued coefficient at the lth tap. $\delta_K(n)$ is the unit impulse function. Assume an STO denoted by θ to be an integer number of the sampling period T, the received signal can be expressed as

$$r_n = e^{j\frac{2\pi\varepsilon n}{N}} \cdot \sum_{l=\theta}^{\theta+L} a_{l-\theta} \cdot s_{n-l} + v_n, \tag{2}$$

where ε is the CFO normalized to the carrier spacing $\frac{1}{T_\mathrm{s}}$. The additive white Gaussian noise is referred to as v_n.

B. STO Estimator based on an Energy Transition Metric

In [9], a difference metric is defined as

$$d_n = \mathbb{E}\left\{ \Big| \, |r_n| - |r_{n-N}| \, \Big|^2 \right\}. \tag{3}$$

Given the received signal model in Equation (2), the difference metric d_n for $n \in [L, N + N_\mathrm{g} + L - 1]$ can be expressed as in Equations (4)-(7). The average signal(noise) power is denoted by $\sigma_s^2(\sigma_v^2)$.

Due to the property of the CP-OFDM, every ISI-free region in the CP delivers a minimum of the difference metric (6). The variation of the difference metric is depicted illustratively in Figure 1. After this ISI-free region, a new OFDM symbol starts.

In order to detect this transition point, an energy transition metric based on the difference metric is defined in [9] as

$$M(n) = \frac{d_n}{d_{n-1}}. \tag{8}$$

Then, a blind symbol timing estimator can be expressed as

$$\hat{\theta} = \arg\max_n M(n) = \arg\max_n \frac{d_n}{d_{n-1}}, \tag{9}$$

with $\hat{\theta} \in \{L, \ldots, N + N_\mathrm{g} + L - 1\}$. At the optimal symbol timing position $\theta = N + N_\mathrm{g}$, there is

$$M(N + N_\mathrm{g}) = \frac{d_{N+N_\mathrm{g}}}{d_{N+N_\mathrm{g}-1}} = \frac{|a_0|^2\sigma_s^2 + \sigma_v^2}{\sigma_v^2}. \tag{10}$$

This method shows good performance against frequency selective fading channels which have large delay spread even for the case $L > N_\mathrm{g}$. However, in the low SNR regime, as shown in Equation (10), the signal that arrived through the first channel tap is severely corrupted by noise.

C. Modified Symbol Timing Estimator

In this section, a modified transition metric for the symbol timing estimator is presented.

Instead of Equation (8), we define $M'(n)$ based on multiple observations of the difference metric d_n, given by

$$M'(n) = \frac{\sum_{k=0}^{K-1} d_{n+k}}{\sum_{k=0}^{K-1} d_{n-k-1}}. \tag{11}$$

When $K \leq N_\mathrm{g} - L$, we obtain at the ideal symbol timing position $\theta = N + N_\mathrm{g}$

$$M'(N + N_\mathrm{g}) = \frac{\sigma_s^2 \sum_{k=0}^{K-1}(K-k)|a_k|^2 + K\sigma_v^2}{K\sigma_v^2}. \tag{12}$$

Equation (12) implies that the selection of K depends on the maximum channel delay L. Details of this issue will be discussed in Section III-A.

III. Discussion

In this section, we discuss several aspects regarding the energy transition metric based symbol timing estimator.

A. Selection of K

In order to find the optimal K in Equation (11), we simulate the Signal-to-Interference-and-Noise-Ratio (SINR) after the FFT on the receiver side. For each channel realization at each SNR, different values of K are applied to Equation (11) to estimate the STO. The post-FFT SINR loss shown in Figure 2 can be interpreted as the ICI/ISI introduced by the STO estimation errors. Similar SINR results can also be calculated using the mathematical analysis in [3].

In Figure 2, it can be observed that in the high SNR region, the lowest SINR loss is obtained when $K = N_\mathrm{g} - L$ is selected. While in the low SNR region, the SINR loss does not increase even if larger values of K are chosen.

B. Estimate the Maximum Channel Delay

As illustrated in Figure 2, in order to achieve lower loss in terms of the post-FFT SINR for all SNR levels, it is necessary to adjust the K according to the maximum channel delay L in the high SNR regime. We exploit the energy transition metric in Equation (8) to estimate L. Given the transition metric $M(n)$, the maximum channel delay can be found by

$$\hat{L} = N_\mathrm{g} - |p_1 - p_2|, \tag{13}$$

where p_i is the argument that delivers the ith maximum of the logarithm of the transition metric

$$\tilde{M}(n) = \ln M(n) = \ln d_n - \ln d_{n-1}. \tag{14}$$

As an example, an evaluated logarithm of the transition metric curve is shown in Figure 3. The two peaks at p_1 and p_2 correspond to the two sharp edges to the ISI-free region in Figure 1.

Since wrong estimations of L typically occur in the low SNR region where the system does not benefit much from the knowledge of L (Figure 2), we choose the factor K to be the CP length in this region. Thus, the selection of K in Equation (11) can be summarized as

$$K = \begin{cases} N_\mathrm{g} - \hat{L}; & \hat{L} < N_\mathrm{g} \\ N_\mathrm{g}; & \text{else} \end{cases} \tag{15}$$

Also, the knowledge of the maximum channel delay spread can be utilized to reduce the computational complexity of the channel estimation effectively, as mentioned in [12, 13].

C. Extension to Multiple Antenna Receiver

Given multiple incoming signals from the multiple receive antenna, the antenna index (m) is introduced into the difference metric:

$$d_n^{(m)} = \mathbb{E}\left\{ \Big| \, |r_n^{(m)}| - |r_{n-N}^{(m)}| \, \Big|^2 \right\}, m = 1, \ldots, N_\mathrm{R}. \tag{16}$$

Correspondingly, the transition metric in Equation (8) becomes

$$\hat{\theta} = \arg\max_n \frac{\sum_{m=1}^{N_\mathrm{R}} \sum_{k=0}^{K-1} d_{n+k}^{(m)}}{\sum_{m=1}^{N_\mathrm{R}} \sum_{k=0}^{K-1} d_{n-k-1}^{(m)}}. \tag{17}$$

$$d_n = \begin{cases} 2\left(\sum_{l=0}^{L} |a_l|^2\sigma_s^2 + \sigma_v^2\right), & L \le n < N \quad (4) \\ 2\left(\sum_{l=n-N}^{L} |a_l|^2\sigma_s^2 + \sigma_v^2\right), & N \le n \le N+L \quad (5) \\ 2\sigma_v^2, & N+L < n < N+N_\mathrm{g} \quad (6) \\ 2\left(\sum_{l=0}^{n-N-N_\mathrm{g}} |a_l|^2\sigma_s^2 + \sigma_v^2\right), & N+N_\mathrm{g} \le n < N+N_\mathrm{g}+L-1 \quad (7) \end{cases}$$

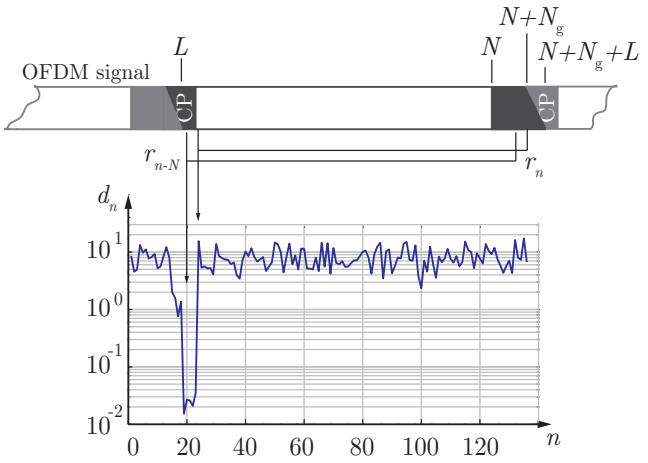

Fig. 1. Difference metric d_n.

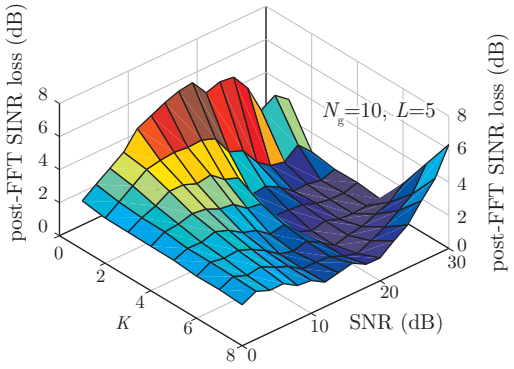

Fig. 2. post-FFT SINR loss.

D. Robustness to Carrier Frequency Offset

In a practical system, the symbol timing needs to be acquired prior to all other operations in the receiver. The received OFDM signal might be disturbed by a CFO which is expressed as an additional exponential term in Equation (2). Therefore, it is crucial that a symbol timing estimator is robust against a large CFO.

Since the difference metric in Equation (3) merely considers the amplitude of the received signal, the influence of the CFO is excluded.

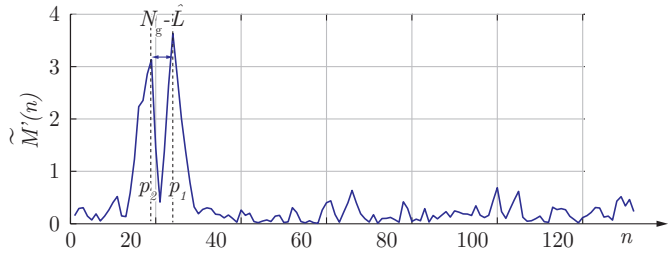

Fig. 3. Maximum channel delay estimation.

TABLE I
SIMULATION PARAMETERS

Parameter	Value
Bandwidth	1.4 MHz
FFT size (N)	128
CP length (N_g)	normal (10) [17]
Subcarrier spacing	15 kHz
Transmission setting	1×1, 2×2
Transmission mode	open loop spatial multiplexing
Channel model	ITU PedB [18]
Symbol timing offset	$0/23T \approx 12\,\mu s$
Carrier frequency offset	$0/3.1415$ subcarrier spacings
Channel estimation	Least Squares
Receiver type	soft sphere decoder

IV. SIMULATIONS

In this section, we compare the performance of the modified STO estimator with the original method presented in [9]. All simulation results are obtained using a Matlab-based LTE link level simulator [16] which has an OFDM physical layer. All scripts can be downloaded from [15]. The simulation parameters are summarized in Table I.

A. Estimation Performance

The estimation performance achieved by the mentioned estimators is evaluated in terms of lock-in probability P_l in Figure 4. It is defined as the probability that the symbol timing error is within the region $(L - N_\mathrm{g}) \le (\hat{\theta} - \theta) \le 0$. In this simulation, K is fixed to $N_\mathrm{g} - L$.

As a reference, we plot the lock-in probability of the autocorrelation based STO estimator proposed in [8] for the

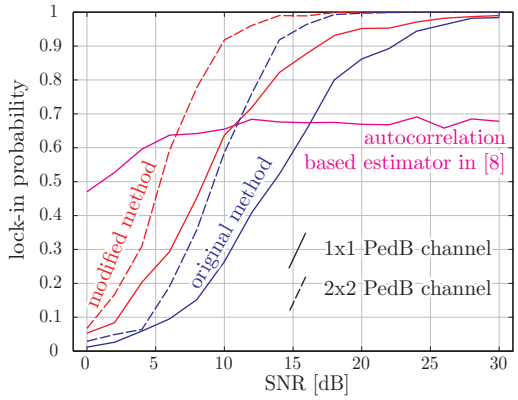

Fig. 4. Lock-in probability P_l

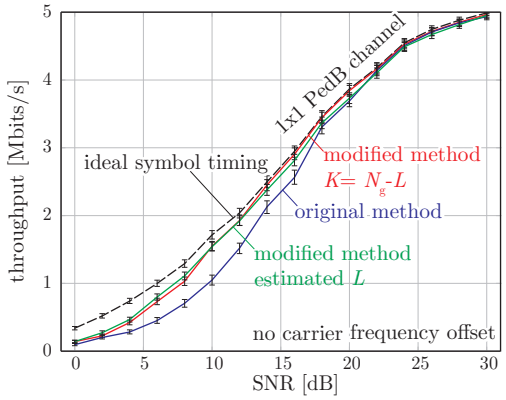

Fig. 5. Modified STO estimator with estimated maximum channel delay L

SISO case. Because it suffers the drawback that the strongest channel path is recognized instead of the first, the curve saturates at a certain SNR. However, the original transition metric based method merely shows an advantage for SNRs higher than 16 dB. Our modified method enables this cross point below approximately 11 dB. In a practical SNR region between 10 dB and 15 dB, symbol timing can be acquired more accurately.

B. Coded Throughput

In addition to the estimation error probability, we evaluate the coded throughput of the physical layer when imperfect symbol timing is considered. Adaptive modulation and coding schemes are implemented using an optimal feedback. Using the bootstrap algorithm [19] we calculated the 95% confidence intervals for all simulated curves. These intervals are indicated by the vertical bars in the simulated curves.

In Figure 5, we investigate the influence of different values of K on the system performance for the single antenna case. With the estimated maximum channel delay described in Section III-B, the modified estimator shows a throughput close to that with the optimal value of K. Therefore, in the following simulation, we fixed K to $N_\mathrm{g} - L$.

In Figure 6, the modified estimator shows considerable improvements in throughput compared to the original method when the SNR is lower than 15 dB. In Figure 7, we plot the throughput loss caused by imperfect OFDM symbol timing. At a typical SNR of 10 dB, the modified method brings the loss from 40 % down to 10 % for the SISO case and 15 % to 0 for the MIMO case.

In Figure 8, imperfect symbol timing and carrier frequency synchronization are both taken into account. Symbol timing is acquired using our modified transition metric based method. The CFO is estimated and compensated using the approach presented in [20]. As expected in Section III-D, the transition metric based STO estimator is robust against large CFOs.

V. Conclusion

In this paper, we presented an STO estimator using a modified transition metric. Simulation results show that the modified method provides considerable improvements in terms of estimation performance and system throughput in a low to medium SNR region compared to the original transition metric based estimator.

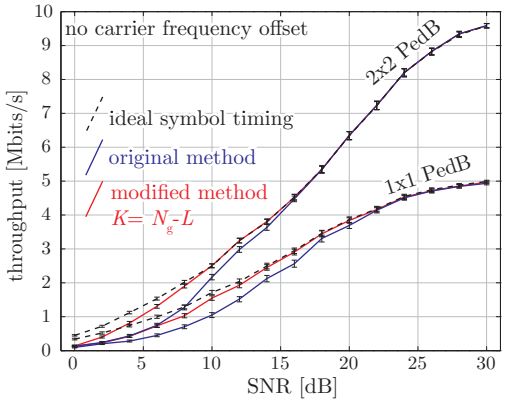

Fig. 6. Coded throughput comparison: ideal symbol timing vs. estimated symbol timing.

Acknowledgments

Funding for this research was provided by the fFORTE WIT - Women in Technology Program of the Vienna University of Technology. This program is co-financed by the Vienna University of Technology, the Ministry for Science and Research and the fFORTE Initiative of the Austrian Government. Also, this work has been co-funded by the Christian Doppler Laboratory for Wireless Technologies for Sustainable Mobility.

References

[1] IEEE, "IEEE standard for local and metropolitan area networks; part 16: Air interface for fixed broadband wireless access systems, IEEE Std. 802.16-2004," Oct. 2004. [Online]. Available: http://standards.ieee.org/getieee802/download/802.16-2004.pdf

[2] 3GPP, "Technical specification group radio access network; (E-UTRA) and (E-UTRAN); overall description; stage 2," Tech. Rep., Sep. 2008. [Online]. Available: http://www.3gpp.org/ftp/Specs/html-info/36300.htm

[3] Y. Mostofi and D. C. Cox, "Mathematical analysis of the impact of time synchronization errors on the performance of an OFDM system," *IEEE Transactions on Communications*, vol. 54, no. 2, pp. 226–230, Feb. 2006.

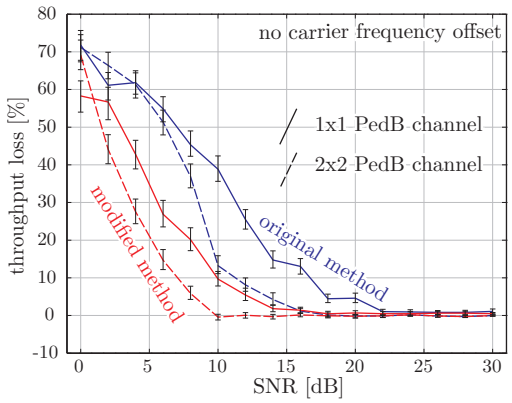

Fig. 7. Coded throughput loss

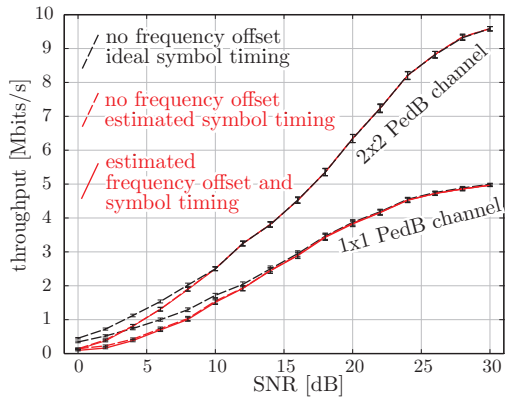

Fig. 8. Imperfect symbol timing and carrier frequency synchronization

[4] M. Speth, F. Classen, and H. Meyr, "Frame synchronization of OFDM systems in frequency selective fading channels," in *IEEE 47th Vehicular Technology Conference*, May 1997, pp. 1807–1811.

[5] T. Schmidl and D. Cox, "Robust frequency and timing synchronization for OFDM," *IEEE Transactions on Communications*, vol. 45, pp. 1613–1621, Dec 1997.

[6] M. Speth, S. Fechtel, G. Fock, and H. Meyr, "Optimum receiver design for OFDM-based broadband transmission. II. a case study," *IEEE Transactions on Communications*, vol. 49, pp. 571–578, Apr 2001.

[7] H. Minn, V. K. Bhargava, and K. B. Letaief, "A robust timing and frequency synchronization for OFDM systems," *IEEE Transactions on Wireless Communications*, vol. 2, no. 4, pp. 822–839, Jul. 2003.

[8] J. J. van de Beek, M. Sandell, and P. O. Borjesson, "ML estimation of time and frequency offset in OFDM system," *IEEE Transactions on Signal Processing*, vol. 45, pp. 1800–1805, Jul. 1997.

[9] V. Le Nir, T. van Waterschoot, J. Duplicy, and M. Moonen, "Blind coarse timing offset estimation for CP-OFDM and ZP-OFDM transmission over frequen cy selective channels," *EURASIP Journal on Wireless Communications and Networking*, vol. 2009, Article ID 262813, 2009.

[10] H. Bölcskei, "Blind estimation of symbol timing and carrier frequency offset in wireless OFDM systems," *IEEE Transactions on Communications*, vol. 49, no. 6, pp. 988–999, Jun. 2001. [Online]. Available: http://www.nari.ee.ethz.ch/commth/pubs/p/synch

[11] R. Mo, Y. H. Chew, T. T. Tjhung, and C. C. Ko, "A new blind joint timing and frequency offset estimator for OFDM systems over multipath fading channels," *IEEE Transactions on Vehicular Technology*, vol. 57, no. 5, pp. 2947–2957, September 2008.

[12] Q. Wang, D. Wu, J. Eilert, and D. Liu, "Cost analysis of channel estimation in MIMO-OFDM for software defined radio," in *Proc. IEEE Wireless Communications & Networking Conference (WCNC 2008)*, Las Vegas, USA, Apr. 2008.

[13] M. Šimko, D. Wu, C. Mehlführer, J. Eilert, and D. Liu, "Implementation Aspects of Channel Estimation for 3GPP LTE Terminals," in *Proc. European Wireless (EW 2011)*, Vienna, Austria, Apr. 2011.

[14] C. Mehlführer, M. Wrulich, J. C. Ikuno, D. Bosanska, and M. Rupp, "Simulating the long term evolution physical layer," in *Proc. 17th European Signal Processing Conference (EUSIPCO 2009)*, Glasgow, Scotland, UK, Aug. 2009. [Online]. Available: http://publik.tuwien.ac.at/files/PubDat_175708.pdf

[15] "LTE simulator homepage." [Online]. Available: http://www.nt.tuwien.ac.at/ltesimulator/

[16] C. Mehlführer, J. C. Ikuno, M. Šimko, S. Schwarz, M. Wrulich, and M. Rupp, "The Vienna LTE Simulators - Enabling Reproducibility in Wireless Communications Research," *EURASIP Journal on Advances in Signal Processing*, 2011.

[17] 3GPP, "Technical specification group radio access network; (E-UTRA) and (E-UTRAN); physical channels and modulation; (release 8)," Tech. Rep., Sep. 2008. [Online]. Available: http://www.3gpp.org/ftp/Specs/html-info/36211.htm

[18] "Recommendation ITU-R M.1225: Guidelines for evaluation of radio transmission technologies for IMT-2000," Tech. Rep., 1997.

[19] B. Efron and D. V. Hinkley, *An Introduction to the Bootstrap (CRC Monographs on Statistics & Applied Probability 57)*, 1st ed. Chapman & Hall/CRC, 1994.

[20] Q. Wang, C. Mehlführer, and M. Rupp, "Carrier frequency synchronization in the downlink of 3GPP LTE," in *Proceeding of the 21st Annual IEEE International Symposium on Personal, Indoor and Mobile Radio Communications (PIMRC'10)*, Istanbul, Turkey, Sep. 2010.